

# Born–Haber Cycle for Monolayer Self-Assembly at the Liquid–Solid Interface: Assessing the Enthalpic Driving Force

Wentao Song,<sup>†,‡</sup> Natalia Martsinovich,<sup>§</sup> Wolfgang M. Heckl,<sup>†,‡</sup> and Markus Lackinger<sup>\*,†,‡</sup>

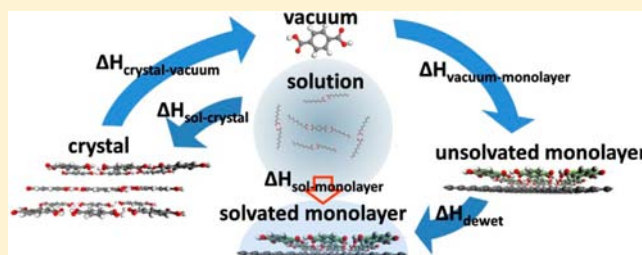
<sup>†</sup>Deutsches Museum, Museumsinsel 1, 80538 Munich, Germany

<sup>‡</sup>TUM School of Education, Technical University Munich, Schellingstrasse 33, 80799 Munich, Germany

<sup>§</sup>Department of Chemistry, University of Warwick, Coventry CV4 7AL, U.K.

## S Supporting Information

**ABSTRACT:** The driving force for self-assembly is the associated gain in free energy with decisive contributions from both enthalpy and entropy differences between final and initial state. For monolayer self-assembly at the liquid–solid interface, solute molecules are initially dissolved in the liquid phase and then become incorporated into an adsorbed monolayer. In this work, we present an adapted Born–Haber cycle for obtaining precise enthalpy values for self-assembly at the liquid–solid interface, a key ingredient for a profound thermodynamic understanding of this process. By choosing terephthalic acid as a model system, it is demonstrated that all required enthalpy differences between well-defined reference states can be independently and consistently assessed by both experimental and theoretical methods, giving in the end a reliable value of the overall enthalpy gain for self-assembly of interfacial monolayers. A quantitative comparison of enthalpy gain and entropy cost reveals essential contributions from solvation and dewetting, which lower the entropic cost and render monolayer self-assembly a thermodynamically favored process.



## INTRODUCTION

Supramolecular self-assembly has been extensively studied for gaining a fundamental understanding of its mechanisms and driving forces.<sup>1–5</sup> This knowledge provides the basis for the efficient and targeted bottom-up fabrication of functional nanostructures. Among the different environments and dimensionalities for self-assembly, two-dimensional surface-supported monolayers take a special role. On the one hand, adsorption on solid substrates readily provides an interface and support for the structures, an important prerequisite for applications in sensors and catalysis.<sup>6–8</sup> On the other hand, surface-supported monolayers are ideal model systems since their properties become analytically accessible by established techniques, such as scanning probe microscopy.<sup>9–12</sup> Liquid environments are of particular interest because they enable facile preparation but also serve as suitable test grounds for biological environments. In addition, liquid environments mediate high mobility of the molecular building blocks and enhance bond reversibility. Consequently, many self-assembled structures represent the thermodynamic equilibrium.<sup>9,11–14</sup> This holds especially true for supramolecular monolayers at the liquid–solid interface, where thermodynamical descriptions were extremely successful for understanding structure formation and transitions, even in complex multicomponent systems. Thermodynamic models that utilize the concentration dependence of chemical potentials can explain the emergence of different phases with different surface packing densities as a function of solute concentration in homomeric systems<sup>15,16</sup> and

the emergence of different phases with different packing densities and compositions as a function of the two solute concentrations in bimolecular systems.<sup>17</sup> In an alternative approach, the free energy of monolayer self-assembly is estimated by separate evaluation of its contributions, i.e., the enthalpy gain and the entropy loss. Using this approach, it was possible to understand the driving force for temperature-induced reversible phase transitions<sup>18</sup> and the emergence of phases with nonideal, untypical hydrogen-bonding motifs in tricarboxylic acid monolayers.<sup>19</sup> On the other hand, Bellec et al. demonstrated that kinetic effects can also become important.<sup>20</sup> All these thermodynamic models provide rationales to understand structure selection but do not facilitate more detailed insight in the subtle balance of the various individual enthalpy and entropy contributions. Only such an in-depth understanding will result in a full quantitative thermodynamical picture of self-assembly, an important step toward deliberate control of nanostructure formation by self-assembly.

Monolayer self-assembly at the liquid–solid interface is driven by the free energy difference between the final state, where molecules are adsorbed and incorporated into the interfacial monolayer, and the initial state, where molecules are dissolved in the supernatant solution. In comparison to self-assembly at the vacuum–solid interface, the presence of the supernatant liquid phase has profound consequences. For

Received: July 26, 2013

Published: September 4, 2013

instance, the substrate may be precovered with solvent molecules, and desorption of this wetting layer causes an additional enthalpy cost.

Because of the complexity of the solid-monolayer-liquid system and the various adsorption and desorption processes taking place at this interface, a precise quantification of the overall enthalpy difference of self-assembly can become intricate. In principle, microflow calorimetry (MFC) is an established technique to measure adsorption enthalpies from solution on graphitic supports.<sup>21</sup> To amplify the measured heat, MFC takes advantage of large surfaces, as available in graphon (graphitized carbon black). Despite the many advantages of MFC, such as its straightforwardness and the low instrumental effort, several drawbacks remain. First, it is not parameter-free, since the normalization of adsorption energies requires a precise measurement of the surface area, as typically obtained from gas adsorption experiments, which are also not parameter-free. MFC is inherently limited to materials with large specific areas of distinct crystallographic surfaces (although this is less of a problem for graphitic materials, thanks to the availability of well-defined (0001) facets). Furthermore, the method is of limited use for processes with particularly small enthalpy differences because the accuracy decreases with the overall enthalpy.

As an alternative route for obtaining the overall enthalpy difference, we present the implementation of a Born–Haber cycle for interfacial monolayer self-assembly. This approach circumvents the above-mentioned disadvantages of MFC, and in addition not only the overall enthalpy is obtained but individual enthalpy contributions are evaluated, thereby offering detailed fundamental insights into the subtle thermodynamic balance of monolayer self-assembly. Moreover, the influence of the solvent can be better understood. This is particularly important because the solvent can play a key role in controlling the monolayer structure in the systems where polymorphism is possible.<sup>22–24</sup>

Widely studied terephthalic acid (TPA, 1,4-benzenedicarboxylic acid) has been chosen as a generic model system because hydrogen-bonded networks are among the most important classes of interfacial monolayers. In addition, self-assembly of TPA was already experimentally studied on a variety of different surfaces<sup>25–30</sup> and theoretically by Monte Carlo simulations.<sup>31,32</sup> Moreover, TPA is conformationally rigid, and its relatively small size permits more elaborate calculations as pursued here. However, until now no detailed quantitative thermodynamic understanding of TPA monolayer self-assembly from solution has been realized.

In this work, we combine the results from an array of experimental techniques to provide a detailed quantitative picture of all significant enthalpy contributions. In addition, all enthalpy contributions were independently assessed by molecular mechanics (MM) and molecular dynamics (MD) simulations based on the MM3 force field.<sup>33–35</sup> TPA bulk crystals, unsolvated TPA monolayers, isolated molecules in the gas phase, and dissolved molecules in nonanoic acid (9A) solution serve as well-defined and easily accessible reference states, both for experiments and theoretical calculations. Precise knowledge of the decisive overall enthalpy change enables a quantitative comparison with the entropy cost of self-assembly as obtained from established theoretical models.<sup>36</sup> Contrasting enthalpy gain and entropy cost reveals essential contributions from both solvation and wetting (or dewetting) the substrate

by solvent molecules, which crucially affect both the enthalpy and the entropy balance.

## METHODS

**Experimental Section.** The sublimation enthalpy was derived by measurements of the effusion rate that is proportional to the saturated vapor pressure for different temperatures. To this end, an effusion cell equipped with a quartz crystal microbalance was used in high vacuum.<sup>37</sup> Constant slopes in the shift of resonant frequency ( $\Delta f$ ) vs time ( $t$ ) traces for all temperatures indicate the validity of the chosen approach.

TPA solubility, i.e., the saturation concentration, was determined by temperature-dependent UV–vis absorption spectroscopy using spectra of pure 1-nonanoic acid (9A) solvent at the respective temperatures as reference. According to Lambert–Beer's law, the concentration is directly proportional to the absorbance. UV–vis absorption spectra of TPA exhibit two clear absorption bands centered at 290 and 300 nm due to  $n-\pi^*$  and  $\pi-\pi^*$  transitions as anticipated for an aromatic compound. Since there is no interference with absorption of the 9A solvent in this spectral range, temperature-dependent UV–vis absorption spectroscopy is very well suited to quantify the enthalpy of dissolution.

Temperature programmed desorption (TPD) experiments were conducted in ultrahigh vacuum. TPA monolayers were first deposited onto a graphite surface by thermal sublimation. Subsequently, the sample temperature was ramped up linearly in time, and the TPA desorption rate was simultaneously recorded by a mass spectrometer. Three sets of experiments were performed with three different heating rates ranging from 0.25 to 0.84 K s<sup>-1</sup>. The complete analysis method was used to derive the desorption enthalpy because no a priori assumptions either on the desorption order or on the underlying desorption mechanism are required.<sup>38</sup>

**Computational.** Molecular mechanics and molecular dynamics calculations were conducted using the MM3 force field.<sup>33–35</sup> The strength of the 2-fold hydrogen bonds between carboxylic acid groups is considerably enhanced by resonance effects.<sup>39,40</sup> So-called resonance-assisted hydrogen bonds (RAHB) can occur when the hydrogen bond donor and acceptor are connected by a short  $\pi$ -conjugated segment such as C=O in carboxylic groups. Then enhancement of the  $\pi$ -delocalization synergistically increases the hydrogen bond strength. Thus, in order to obtain accurate enthalpy values for hydrogen bonds, the MM3 force field was modified accordingly.<sup>31</sup>

The lowest energy TPA bulk structure was found by first optimizing the lattice parameters  $A$ ,  $B$ , and  $\gamma$  for the 2D lattice and then using them as a starting point for optimizing the lattice parameters  $C$ ,  $\alpha$ , and  $\beta$ . The calculated lattice parameters for the optimized triclinic TPA crystal were:  $A = 9.37 \text{ \AA}$ ,  $B = 7.70 \text{ \AA}$ ,  $C = 3.56 \text{ \AA}$ ,  $\alpha = 83^\circ$ ,  $\beta = 74^\circ$ ,  $\gamma = 131^\circ$ , in good agreement with the X-ray crystal structure (form I):  $A = 9.54 \text{ \AA}$ ,  $B = 7.73 \text{ \AA}$ ,  $C = 3.74 \text{ \AA}$ ,  $\alpha = 109^\circ 9'$ ,  $\beta = 73^\circ 36'$ ,  $\gamma = 137^\circ 46'$ .<sup>41</sup>

A theoretical estimate for the enthalpy of dissolution was obtained from MD simulations of TPA molecules surrounded by 200 solvent molecules in a periodic box. The annealed solvent structure was used as a starting point for building a model of TPA in solution and for the following MD simulations. To create a model of TPA in solution, either one TPA molecule was added to the system of 200 annealed 9A molecules (two “added TPA” structures were used) or one of the 9A molecules was removed and replaced with TPA (four “substituted TPA” structures were used). The MD simulations of the pure solvent and of TPA in solution were conducted using the MM3 force field and, independently, using the CHARMM force field.<sup>42</sup>

## RESULTS AND DISCUSSION

**Monolayer Structure.** The TPA monolayer structure at the 9A–graphite interface was determined by in situ Scanning Tunneling Microscopy (STM) experiments, a high-resolution image is depicted in Figure 1. Precise unit cell parameters were obtained by calibration with the underlying graphite lattice.

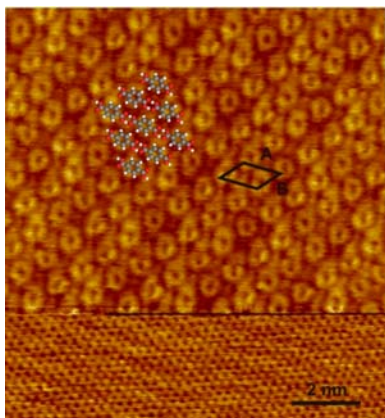


**Figure 1.** STM image of a TPA monolayer at the nonanoic acid–graphite interface. The lower part the graphite substrate was imaged with atomic resolution by decreasing the tunneling gap. With this internal calibration standard precise lattice parameters for the TPA monolayer of  $A = (9.6 \pm 0.1) \text{ \AA}$ ,  $B = (7.8 \pm 0.1) \text{ \AA}$ , and  $g = 130^\circ \pm 1^\circ$  were deduced. The arrangement of TPA molecules is indicated by the overlay, and the black lines mark the unit cell (image size  $10.9 \times 10.2 \text{ nm}^2$ ,  $I = 100 \text{ pA}$ ,  $V_{\text{sample}} = -80.0 \text{ mV}$  for TPA;  $I = 200 \text{ pA}$ ,  $V_{\text{sample}} = -1.53 \text{ mV}$  for graphite).

TPA forms well-ordered densely packed monolayers with lattice parameters  $A = (9.6 \pm 0.1) \text{ \AA}$ ,  $B = (7.8 \pm 0.1) \text{ \AA}$ ,  $\gamma = 130^\circ \pm 1^\circ$  and one molecule per unit cell. As indicated by the overlay, the monolayer structure consists of densely packed linear hydrogen bonded chains, where TPA molecules are interconnected by 2-fold cyclic hydrogen bonds between the carboxyl groups. The STM contrast always exhibited a Moiré pattern indicating a weak interaction between TPA and graphite and incommensurability of the superstructure with the graphite lattice.

**Born–Haber Cycle.** The overall enthalpy change of TPA monolayer self-assembly is evaluated by the adapted Born–Haber cycle depicted in Figure 2. The well-defined reference states are TPA bulk crystal, unsolvated TPA monolayer, isolated single TPA molecules in vacuum, and solvated single TPA molecules in 9A solution. Since the graphite substrate is initially precovered by an ordered 9A solvent wetting layer (cf. Supporting Information), the enthalpy cost of dissolution of the

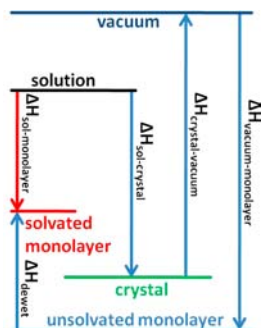


**Figure 2.** Scheme of the proposed Born–Haber cycle.  $\Delta H_{\text{sol}\rightarrow\text{monolayer}}$  (red arrow) is not directly accessible, but a detour via crystal, vacuum, and unsolvated monolayer (blue arrows) facilitates quantification of the overall enthalpy difference. There is a notable enthalpy difference for the monolayer at the vacuum–solid interface (“unsovlated monolayer”) as compared to the liquid–solid interface (“solvated monolayer”) due to solvent contributions.

9A wetting layer and the enthalpy gain due to solvation of the adsorbed TPA monolayer by the solvent are taken into account by a dewetting enthalpy  $\Delta H_{\text{dewet}}$ . Hence, knowledge of the sublimation enthalpy ( $\Delta H_{\text{crystal}\rightarrow\text{vacuum}}$ ), desorption enthalpy from the unsolvated monolayer into vacuum ( $\Delta H_{\text{monolayer}\rightarrow\text{vacuum}}$ ), the enthalpy of dissolution ( $\Delta H_{\text{crystal}\rightarrow\text{sol}}$ ) and dewetting enthalpy  $\Delta H_{\text{dewet}}$  enables one to indirectly conclude on the decisive overall enthalpy difference between solution and solvated monolayer ( $\Delta H_{\text{sol}\rightarrow\text{monolayer}}$ ):

$$\begin{aligned} \Delta H_{\text{sol}\rightarrow\text{monolayer}} &= \Delta H_{\text{sol}\rightarrow\text{crystal}} + \Delta H_{\text{crystal}\rightarrow\text{vacuum}} \\ &\quad + \Delta H_{\text{vacuum}\rightarrow\text{monolayer}} + \Delta H_{\text{dewet}} \\ \Delta H_{\text{sol}\rightarrow\text{monolayer}} &= -\Delta H_{\text{crystal}\rightarrow\text{sol}} + \Delta H_{\text{crystal}\rightarrow\text{vacuum}} \\ &\quad - \Delta H_{\text{monolayer}\rightarrow\text{vacuum}} + \Delta H_{\text{dewet}} \quad (1) \end{aligned}$$

The first three terms on the right-hand side of eq 1 refer to the experimentally measured enthalpy differences. There it was considered that permutation of initial and final state inverts the sign. In the following it will be demonstrated that all TPA-related enthalpy differences can independently and consistently be assessed by both experimental and theoretical approaches.

**Sublimation Enthalpy.** The sublimation enthalpy is derived from temperature-dependent measurements of the effusion rate of TPA with a quartz crystal microbalance in the range between 100 and 120 °C in high vacuum. The effusion rate is proportional to the saturated vapor pressure, thereby providing access to the related thermodynamic quantity. The corresponding Van’t Hoff plot in Figure 3b yields a sublimation enthalpy of  $\Delta H_{\text{crystal}\rightarrow\text{vacuum}} = +(127.2 \pm 3.6) \text{ kJ/mol}$ . TPA sublimation is a strongly endothermic process because bonds within the crystal are broken and single molecules cannot regain this enthalpy in the gas phase. In these kinetic experiments, the sublimation rates of TPA monomers are measured, and a conceivable subsequent dimerization in the gas phase does not affect the experimental result.

The binding energy of TPA in the crystal with respect to vacuum was also calculated by molecular mechanics (MM, cf. Methods and the Supporting Information for details). The theoretical evaluation of the sublimation enthalpy relies on the computational search for the lowest-energy TPA bulk crystal structure by varying all lattice parameters and taking the experimental X-ray structure into account as an initial guess.<sup>41</sup> Thus, the aim was not to predict all possible TPA polymorphs, but to verify that the MM description of the TPA crystal structure is accurate and reliably reproduces the experimental structure. The calculated value of the crystal binding energy  $-129.1 \text{ kJ/mol}$  is in excellent agreement with the measured sublimation enthalpy of  $+127.2 \text{ kJ/mol}$ . This confirms the suitability of MM simulations and the MM3 force field (with appropriately modified hydrogen bond energy parameters<sup>31</sup>) for a reliable quantitative assessment of enthalpies in resonance enhanced hydrogen bonded structures.

**Enthalpy of Dissolution.** In a similar way, solubility measurements of TPA in 9A as a function of temperature yield the enthalpy of dissolution  $\Delta H_{\text{crystal}\rightarrow\text{sol}}$ . UV–vis absorption spectra of TPA in 9A were acquired between 30 and 42 °C and are shown in Figure 4a. For the Van’t Hoff plot depicted in Figure 4b the total amount of dissolved TPA molecules was estimated by integrating the absorbance vs  $\lambda$  curves over the absorption band, yielding an enthalpy of dissolution of  $+(12.8 \pm 1.3) \text{ kJ/mol}$ . The positive enthalpy of dissolution indicates

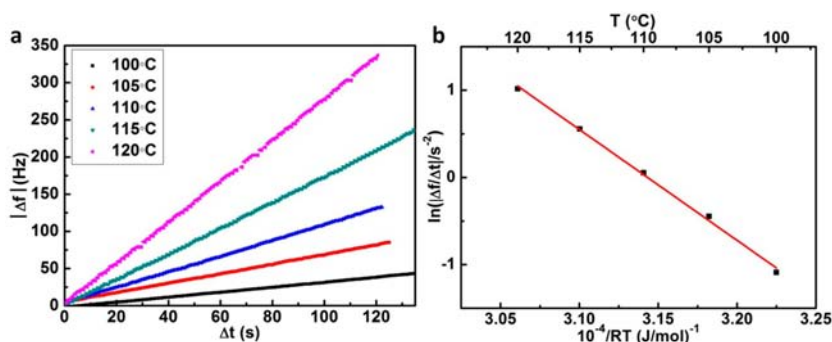


**Figure 3.** Measurement of the TPA effusion rate as a function of temperature: (a) resonant frequency shift  $\Delta f$  of the quartz crystal microbalance vs time traces for different temperatures of the effusion cell; (b) corresponding Van't Hoff plot; each data set in (a) was fitted with a straight line and is represented by one data point. The slope corresponds to a sublimation enthalpy of  $+(127.2 \pm 3.6)$  kJ/mol.

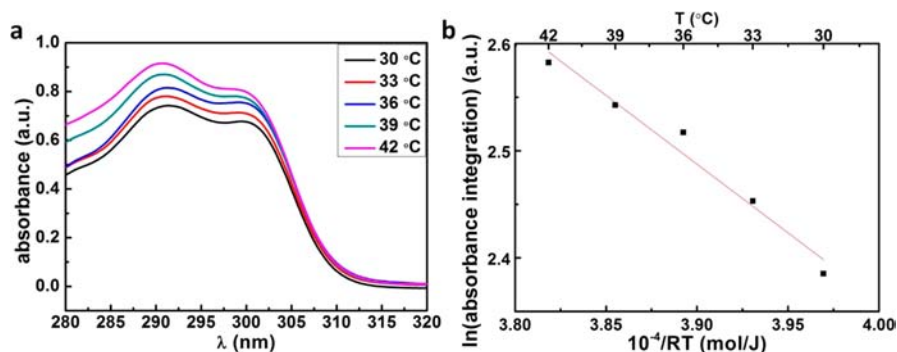


**Figure 4.** Measurement of the TPA solubility in 9A as a function of temperature: (a) UV-vis absorption spectra of saturated TPA in 9A solutions obtained at different temperatures; (b) Van't Hoff plot of the absorbance integrated in the interval  $\lambda = 290$  nm-320 nm. The slope yields a value for the enthalpy of dissolution of  $+(12.8 \pm 1.3)$  kJ/mol.

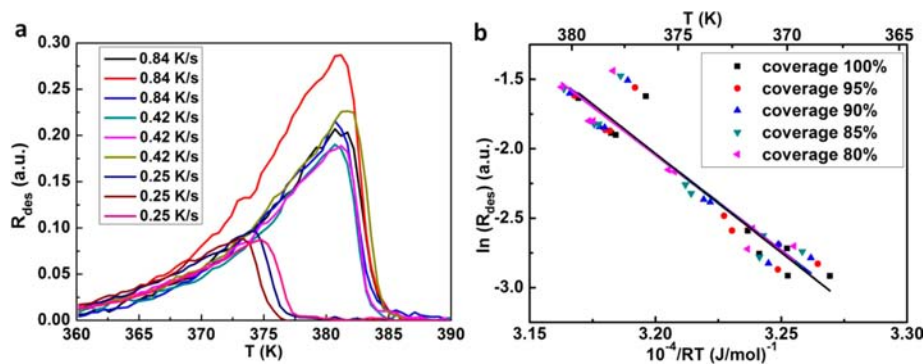


**Figure 5.** Temperature programmed desorption of TPA from graphite in ultrahigh vacuum: (a) desorption rate vs sample temperature traces for different heating rates; (b) corresponding plot obtained from a complete analysis of the desorption traces. The enthalpy of desorption amounts to  $+(140.2 \pm 9.5)$  kJ/mol.

again an endothermic process: the bulk crystal, where TPA molecules are stabilized by hydrogen bonds and additional van der Waals interactions, is the energetically more favorable state. This ideal stabilization is not fully regained in solution and the enthalpic disadvantage corresponds to the measured dissolution enthalpy. However, the dissolution enthalpy is still considerably smaller than the  $-67.8$  kJ/mol binding enthalpy of a 2-fold hydrogen bond between carboxylic acid groups as obtained from infrared absorption spectra of benzoic acid monomer and dimer<sup>40</sup> or from the corresponding computed value  $-67.0$  kJ/mol.<sup>31</sup> From the fact that the endothermic enthalpy of dissolution is still smaller than the binding enthalpy of a hydrogen-bonded carboxylic acid dimer, it is concluded that in the dissolved state TPA is again stabilized by hydrogen bonds:

for statistical reasons, the TPA molecules are most likely surrounded by and bonded to 9A solvent molecules.

Molecular dynamics simulations with the MM3 force field yield an average solvation energy with respect to isolated TPA in vacuum of  $-(115.1 \pm 39.4)$  kJ/mol (cf. Methods and the Supporting Information for details). Additional MD simulations with the CHARMM27 force field<sup>42</sup> yield a value of  $-(118.0 \pm 45.5)$  kJ/mol. The error bars were determined from several independent MD runs and are large because of very slow convergence of energies in MD simulations. The excellent agreement suggests that the MD results do not depend on the choice of force field. We will use the MM3 value for consistency with the other calculations.

Combination of the calculated energy of dissolved TPA with the calculated cohesive energy of the TPA crystal ( $-129.1$  kJ/mol, see the previous subsection) results in a theoretical dissolution enthalpy of  $+14.0$  kJ/mol, in good agreement with the experimental value of  $+12.8$  kJ/mol. Despite the large error bars of the MD simulations, theory and experiment agree that dissolution of TPA in 9A is an endothermic process with a small enthalpy of dissolution.

**Binding Enthalpy of TPA in a Monolayer on Graphite with Respect to Vacuum.** The enthalpy difference between TPA in the monolayer and in the gas phase  $\Delta H_{\text{monolayer} \rightarrow \text{vacuum}}$  is quantified by thermal desorption of TPA from graphite in temperature-programmed desorption (TPD) experiments as illustrated in Figure 5. This established surface science method results in a desorption enthalpy with respect to vacuum of  $(140.2 \pm 9.5)$  kJ/mol.

The theoretical monolayer binding enthalpy was calculated as the sum of independently acquired contributions from molecule–molecule and molecule–substrate interactions. This partition becomes necessary due to the incommensurability of TPA monolayers with the graphite lattice. A further advantage of this approach is the direct comparability of these two contributions. The approach is based on the reasonable assumption that adsorption does not significantly affect the strength of intermolecular bonds.

Theoretical molecule–molecule binding enthalpies were derived for a free-standing TPA monolayer, where optimized lattice parameters were found by scanning through a range of values of  $A$ ,  $B$ , and  $\gamma$ . In good agreement with the experimental unit cell, only one energy minimum was found with  $A = 9.38$  Å,  $B = 8.09$  Å,  $\gamma = 131.5^\circ$ . The binding energy of TPA in the free-standing monolayer was calculated to be  $-76.8$  kJ/mol.

The potential energy for a single TPA molecule on graphite was calculated for a regular grid of different adsorption sites, and the corresponding adsorption energies were found to lie in a narrow range between  $-66.2$  and  $-65.4$  kJ/mol (with the lowest energy and highest energy adsorption configurations corresponding to AB and AA stacking of the benzene ring on the underlying graphite, respectively). The mean value  $-65.8$  kJ/mol is a good approximation for the varying adsorption sites of TPA in the incommensurate superstructure. The small corrugation of the potential energy surface suggests that the underlying graphite does not strongly influence the registry of the TPA monolayer, as also experimentally corroborated by the Moiré pattern.

Combining the adsorption energy with the monolayer binding energy, the theoretical value for the binding enthalpy of TPA in the monolayer on graphite with respect to vacuum is  $-142.6$  kJ/mol, again in perfect agreement with the experimental desorption enthalpy.

**Dewetting Enthalpy.** The aliphatic 9A solvent molecules have a high affinity to graphite and likewise form stable ordered monolayers at the liquid–solid interface at room temperature as confirmed by STM imaging (cf. Supporting Information). The fatty acid monolayer structures are comprised of lamellae of dimers in the all-trans conformation.<sup>43</sup> Initially, this 9A monolayer forms rapidly, and self-assembly of TPA monolayers requires desorption of this solvent wetting layer. MM calculations of the 9A monolayer desorption enthalpy with respect to vacuum yield a value of  $105.7$  kJ/mol, in perfect agreement with the experimental value of  $107.5$  kJ/mol as obtained from TPD experiments.<sup>11,44</sup> When the TPA monolayer is adsorbed at the graphite/solvent interface, the

upper side of the monolayer is exposed to the solvent and is solvated. There is no experimental evidence of 9A forming an ordered overlayer on top of the TPA monolayer, therefore this 9A overlayer is likely to be disordered and liquid-like. It is difficult to provide precise estimates of the interaction energy at this disordered and dynamic interface, either experimentally or computationally. As the upper estimate of the TPA/9A interaction, we can use the calculated energy of an ordered 9A monolayer above a TPA monolayer,  $-84.0$  kJ/mol according to MM calculations. Combining the enthalpy cost of dewetting the graphite surface with the gain due to solvating the TPA monolayer yields a non-negligible enthalpy cost for dewetting of (at least)  $21.7$  kJ/mol per 9A molecule. Since the enthalpies in the Born–Haber cycle refer to TPA molecules,  $\Delta H_{\text{dewet}}$  is given by:

$$\Delta H_{\text{dewet}} = (\Delta H(9A)_{\text{graphite} \rightarrow \text{vacuum}} - \Delta H(9A)_{\text{TPA} \rightarrow \text{vacuum}}) \times \frac{A_{\text{TPA}}}{A_{9A}} \quad (2)$$

The renormalization factor considers that the area  $A_{9A}$  occupied by one 9A molecule of  $66.5$  Å<sup>2</sup> is slightly larger than the area  $A_{\text{TPA}}$  of  $56.8$  Å<sup>2</sup> occupied by one TPA molecule. Accordingly, the contribution to the total enthalpy from dewetting per TPA molecule amounts to  $\Delta H_{\text{dewet}} = +18.5$  kJ/mol.

**Overall Enthalpy Change for Self-Assembly of Interfacial TPA Monolayers.** Eventually, from a combination of all independently assessed enthalpy differences, the desired value for the overall enthalpy difference  $\Delta H_{\text{solution} \rightarrow \text{monolayer}}$  for TPA monolayer self-assembly from solution can be evaluated according to eq 1. For the experimental Born–Haber cycle we obtain  $-7.3$  kJ/mol and for the theoretical cycle the corresponding value amounts to  $-9.0$  kJ/mol, in remarkable agreement with the experiment. Both cycles with all contributions are summarized in Figure 6. For the first time

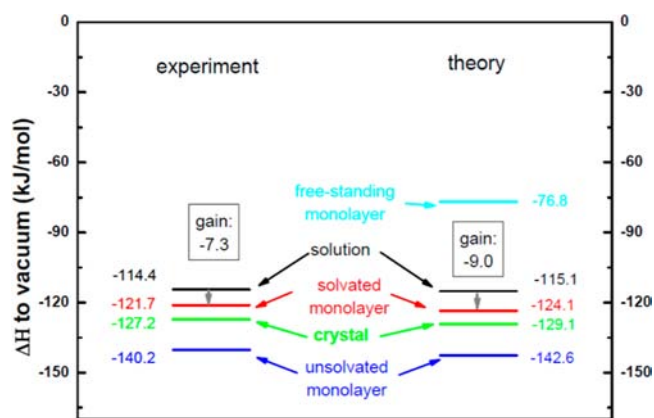


**Figure 6.** Results for the Born–Haber cycle: (left) experimental results; (right) theoretical results; the enthalpy of single TPA molecules in vacuum was used as reference for both theory and experiment.

the substantial lowering of the monolayer desorption enthalpy by the supernatant liquid phase is quantified. It is noteworthy that dewetting the graphite from the initially adsorbed solvent monolayer significantly reduces the enthalpy gain.

For comparison, the enthalpy of desorption of a TPA monolayer from graphite with respect to vacuum is around

+140 kJ/mol, with negligible differences between experiment and theory. With such high desorption barriers spontaneous desorption of TPA at room temperature remains impossible. Even when an extraordinarily high pre-exponential factor of  $10^{18} \text{ s}^{-1}$  is assumed for thermally excited desorption, the corresponding desorption rate at room temperature still remains undetectably low in the order of  $10^{-8} \text{ s}^{-1}$ . Yet, the presence of the solvent significantly lowers the TPA desorption barrier: the value in liquid amounts to only a few percent of the vacuum value. This astonishingly drastic effect is caused by both solvation and solvent wetting. Consequently, thermally stimulated desorption becomes feasible at the liquid–solid interface, whereas it can be fully excluded for the same combination of adsorbate and surface at the vacuum–solid interface. Evidence for desorption even of larger compounds at room temperature at the liquid–solid interface is provided by numerous STM experiments,<sup>45–47</sup> but only here the corresponding enthalpy value has been derived, which for the first time provides a quantitative rationale for this phenomenon.

**Concentration Threshold for Monolayer Self-Assembly.** For spontaneous self-assembly, the enthalpy gain has to overcome the entropy cost, which in solution increases with decreasing solute concentration.<sup>36</sup> This is because the contribution from translational entropy increases with the logarithm of the reciprocal concentration, according to the Sackur–Tetrode equation. Substantial experimental evidence for an increasing entropy cost at lower concentrations is provided by monolayer self-assembly studies at the liquid–solid interface, where either polymorphs with low surface packing densities become favored at lower concentrations<sup>15,19,48,49</sup> or stable monolayer self-assembly is not observed anymore below a certain concentration threshold. Consequently, knowledge of both the overall enthalpy change and the concentration threshold grants experimental access to the entropy cost. For TPA monolayer self-assembly on graphite from 9A solution we find a concentration threshold of  $(120 \pm 15) \mu\text{mol/L}$ .

At the concentration threshold the thermodynamic driving force for monolayer self-assembly vanishes, i.e.,  $\Delta G = 0$ , and consequently,  $\Delta H = T\Delta S$ . Since the enthalpy gain is now precisely known from the Born–Haber cycle, the entropy cost at the concentration threshold can be experimentally quantified and compared to theoretical estimates.

In conclusion, the experimental determination of the concentration threshold for monolayer self-assembly is relatively straightforward but provides important thermodynamical insights. Interestingly, the experimentally determined concentration threshold exceeds the number of TPA molecules required to just cover the graphite surface by a factor of  $\sim 6$ , further evidence for the significance of entropic effects.

**Entropy Cost Vs Enthalpy Gain.** In the following an approach proposed by Whitesides et al. is used to theoretically estimate the entropy balance.<sup>36</sup> Therefore,  $\Delta S$  is partitioned into translational, rotational, vibrational, and conformational entropy. Since TPA is a rigid molecule with only few degrees of freedom, its conformational entropy can be neglected. Also vibrational entropy does not change significantly upon self-assembly and can hence also be disregarded. Further, it is assumed that upon adsorption from solution molecules completely lose their rotational and translational entropy. Accordingly, the total entropy cost  $\Delta S_{\text{rot}}$  of self-assembly is given by the sum of the change (i.e., loss) of rotational entropy  $\Delta S_{\text{rot}} = S_{\text{rot(adsorbed)}} - S_{\text{rot(free)}} = 0 - S_{\text{rot(free)}}$  and the change of translational entropy  $\Delta S_{\text{trans}} = 0 - S_{\text{trans(free)}}$ . The latter depends

on concentration and can be estimated by the Sackur–Tetrode equation:

$$\Delta S_{\text{trans}} = -R \ln \left[ \frac{1}{c} \left( \frac{2\pi m k_{\text{B}} T e^{5/3}}{h^2} \right)^{3/2} \right] \quad (3)$$

Here  $R$  is the gas constant,  $c$  the solute concentration,  $T$  the temperature,  $k_{\text{B}}$  the Boltzmann constant,  $h$  Planck's constant,  $e$  Euler's number, and  $m$  the mass of the molecule. Since it is known that in solutions the use of actual concentrations overestimates  $S_{\text{trans}}$ , free volume corrections were proposed.<sup>36</sup> Here, the concentration of TPA refers to the free volume of 9A as estimated by the hard cube approximation. According to this, the free volume is approximated from the volume difference between two cubes. The volume of the larger cube is obtained from the macroscopic density as the average volume of one solvent molecule, and the volume of the smaller cube corresponds to the van der Waals volume of one solvent molecule. The concentration of the solute is then calculated with respect to the free volume of the solvent, rather than relative to the total volume (i.e., the larger cube) of the solvent.<sup>36</sup>

For evaluation of  $S_{\text{rot}}$  the rigid rotator model was used:

$$\Delta S_{\text{rot}} = -R \ln \left[ \frac{\pi^{1/2}}{\gamma} \left( \frac{8\pi^2 k_{\text{B}} T e}{h^2} \right)^{3/2} (I_1 I_2 I_3)^{1/2} \right] \quad (4)$$

$\gamma$  is related to the rotational symmetry of the solute molecule, i.e., 2 for TPA.  $I_1$ ,  $I_2$ , and  $I_3$  are its principal moments of inertia.

From eqs 3 and 4 the values for  $\Delta S_{\text{trans}}$  and  $\Delta S_{\text{rot}}$  of TPA were calculated and are listed in Table 1. The  $-T(\Delta S_{\text{trans}} + \Delta S_{\text{rot}})$  contribution to  $\Delta G$ , associated with adsorption of a TPA molecule at  $T = 298 \text{ K}$ , amounts to +94.5 kJ/mol.

**Table 1. Contributions of Rotational and Translational Entropy to the Free Energy for Unsolvated TPA Molecules, 9A Dimers, and Hydrogen-Bonded Complexes of TPA and Two 9A Solvent Molecules<sup>a</sup>**

	$c$ ( $\mu\text{mol/L}$ )	$-T\Delta S_{\text{rot}}$ (kJ/mol)	$-T\Delta S_{\text{trans}}$ (kJ/mol)	$-T\Delta S_{\text{tot}}$ (kJ/mol)
TPA	120	+36.7	+57.8	+94.5
9A-9A	$2.84 \times 10^6$	+47.6	+35.2	+82.8
9A-TPA-9A	120	+43.0	+60.9	+103.9

<sup>a</sup>A temperature of 298 K was used.

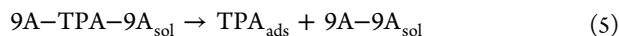
A further entropy contribution arises from dewetting of the graphite, i.e., replacing the solvent wetting layer with the TPA monolayer, because upon desorption 9A molecules regain entropy. This favorable entropic contribution is estimated from the entropy of melting ( $\Delta S_{\text{crystal} \rightarrow \text{liquid}} = 69.5 \text{ J/mol}^{50}$ ) and using the same renormalization factor as in eq 2. This approach assumes that the 9A wetting layer on graphite substrate is ordered (in agreement with 9A lamellae seen by STM), but the 9A wetting layer on TPA monolayer is disordered (liquid-like) and that the entropy difference between 9A in a monolayer and liquid is comparable to the difference between the 9A crystal and liquid. This appears justified, since the main contributions arise from translational, conformational, and rotational entropy that are all zero both in the crystal and in the monolayer. Accordingly, dewetting causes a favorable entropy contribution

of  $-T\Delta S_{\text{dewet}} = -17.7$  kJ/mol (renormalized per 1 TPA molecule). Remarkably, the absolute value of this entropy contribution is only slightly smaller than the renormalized enthalpy cost of dewetting  $\Delta H_{\text{dewet}} = +18.5$  kJ/mol. Accordingly, the enthalpy cost associated with dewetting is almost fully compensated by the entropy gain. Hence, the influence of the solvent wetting layer on  $\Delta G$  is almost negligible.

Yet, the resulting total entropy cost of self-assembly  $-T(\Delta S_{\text{trans}} + \Delta S_{\text{rot}} + \Delta S_{\text{dewet}}) = +76.8$  kJ/mol is significantly larger than the enthalpy gain of  $-7.3$  kJ/mol, as derived from the experimental Born–Haber cycle. According to this estimate, TPA monolayer self-assembly from 9A on graphite should not be thermodynamically favored.

In this simple first approach, however, it was assumed that TPA is dissolved as a single molecule and no further solvation was considered. Yet, such a scenario appears rather unlikely, given that the 9A solvent molecules can likewise form hydrogen-bonded complexes with TPA. It is also well known that fatty acids form hydrogen-bonded dimers in the liquid phase.<sup>51,52</sup> Accordingly, we postulate that solvated TPA molecules form stable, hydrogen-bonded 9A–TPA–9A complexes with two solvent molecules. This assumption is in accord with the low enthalpy of dissolution, indicating that the hydrogen bond stabilization of the crystal is regained in solution as already discussed above. We also evaluated the possibility of the existence of solvated TPA dimers in solution, i.e., the formation of 9A–TPA–TPA–9A complexes, but find that this process is thermodynamically less favorable (cf. the Supporting Information).

Owing to the solvation shell of TPA in 9A, upon adsorption of TPA from solution a 9A–TPA–9A complex is dissociated and the two released 9A molecules recombine into a dimer according to the following scheme:



This solvation also profoundly affects the entropic cost  $\Delta S_{\text{tot}}$  of self-assembly. Both translational and rotational entropy of the 9A–TPA–9A complex are fully lost, but translational and rotational entropy of the 9A–9A dimer are regained.  $\Delta S_{\text{tot}}$  is then given by:

$$\begin{aligned} \Delta S_{\text{tot}} = & \Delta S_{\text{trans}}(9\text{A}-\text{TPA}-9\text{A}) + \Delta S_{\text{rot}}(9\text{A}-\text{TPA}-9\text{A}) \\ & - \Delta S_{\text{trans}}(9\text{A}-9\text{A}) - \Delta S_{\text{rot}}(9\text{A}-9\text{A}) + \Delta S_{\text{dewet}} \end{aligned} \quad (6)$$

All translational and rotational entropies in eq 6 were evaluated according to eqs 3 and 4 using half of the concentration of 9A in pure 9A for the dimer. An all-trans conformation of the alkane chains was assumed for evaluation of the rotational entropy of both the 9A–9A dimer and the 9A–TPA–9A complex. Curling of the alkane chains equally decreases and increases moments of inertia; hence, conformational isomerism has only a minor effect on rotational entropy. All entropies are summarized in Table 1. Accordingly, solvation of TPA by two 9A solvent molecules reduces  $-T\Delta S_{\text{tot}}$  to  $(103.9 - 82.8 - 17.7)$  kJ/mol =  $+3.4$  kJ/mol. This value is in excellent quantitative agreement with the enthalpic gain from the Born–Haber cycle and thus provides substantial evidence that both solvation and dewetting are major contributions for reduction of the entropy cost of self-assembly.

## CONCLUSION AND SUMMARY

An adapted Born–Haber cycle was employed to deduce not only the overall enthalpy change for self-assembly of TPA monolayers at the nonanoic acid–graphite interface but also the individual enthalpy contributions of the various interactions involved in this process. In their initial state, TPA molecules are solvated in 9A and then become incorporated in the interfacial monolayer as their final state. Since the associated overall enthalpy change is particularly small, and thus experimentally difficult to assess by calorimetric methods, a detour was taken via well-defined reference states with accessible enthalpy differences. To this end, enthalpy differences between crystal and gas phase, crystal and solution, as well as monolayer and gas phase were both measured and evaluated by MM and MD simulations. For all enthalpy differences the agreement between experiment and theory is remarkable, thereby providing high confidence in the reliability and accuracy. Since the graphite substrate is initially covered by an ordered 9A solvent monolayer, a further enthalpy contribution arises from dewetting and was estimated by MM simulations.

The most surprising result is that the effective driving force, the enthalpy difference between a self-assembled monolayer and an initially solvent-covered substrate and dissolved TPA molecules, is astonishingly low due to an efficient stabilization of TPA in solution and the enthalpy cost of dewetting. Consequently, the supernatant liquid phase considerably lowers the TPA desorption barrier to only a few percent of the corresponding vacuum desorption barrier. Therefore, for the first time a quantitative rationale is provided for abundantly observed phenomena at the liquid–solid interface that are associated with the vertical mobility of adsorbed molecules, i.e., the possibility of desorption, even of larger compounds at room temperature.<sup>45–47</sup>

The precise quantification of the enthalpic driving force also enables a quantitative comparison with the entropy change of self-assembly as estimated by an established partition scheme. This comparison reveals that solvation through formation of hydrogen-bonded solute–solvent complexes is an important contribution to lowering the entropy cost. Interestingly, a further significant favorable entropic contribution arises from dewetting the substrate because released 9A solvent molecules regain entropy. Entropic contributions are extremely important in self-assembly, and we show that the theoretically estimated entropy cost of self-assembly at thermodynamic equilibrium is in excellent agreement with the overall enthalpy gain, as estimated both by experimental and theoretical methods.

In summary, the liquid phase not only lowers the enthalpy gain of self-assembly, but by the same token also reduces the entropy cost, and thus renders spontaneous self-assembly thermodynamically favorable.

The proposed Born–Haber cycle is widely applicable to many other systems of interest and bears the potential to provide quantitative insights into thermodynamics of self-assembly with a clear recognition of individual enthalpy contributions. Therefore, the role of the solvent can now be clarified on a quantitative basis. The direct comparison pursued here between experiment and theory provides an important benchmarking for simulations. The energetic accuracy obtained here with parametrized force fields is encouraging and opens up venues for studying self-assembly of systems with higher complexity. Hybrid Born–Haber cycles that combine experimental with theoretical results can circumvent problems and

are also more efficient. For instance, larger compounds are thermally less stable and it may not be possible anymore to sublime them as required for sublimation enthalpy measurements or for TPD experiments, but the corresponding binding energies can be assessed computationally. On the other hand, the MD simulations for the enthalpy of dissolution are computationally expensive and time-consuming, whereas temperature dependent experimental UV-vis spectroscopy is relatively straightforward and not restricted by molecular size.

The proposed method is also suitable for studying systems that exhibit solvent-induced polymorphism by evaluating and comparing the free energy gain of the various polymorphs for different solvents. Yet, for systems with phase coexistence, implementation of a Born-Haber cycle might become intricate. In any event, it is important to a priori verify that self-assembly is thermodynamically controlled, for instance by tempering the samples in order to provide thermal energy to overcome kinetic entrapment.<sup>20,24,53</sup>

In conclusion, we show that Born-Haber cycles are a useful and widely applicable tool for a fundamental understanding of the thermodynamics of supramolecular self-assembly. Hybrid Born-Haber cycles constructed from a combination of experiment and simulation are also an efficient method to evaluate thermodynamic contributions for more complex systems.

## ■ ASSOCIATED CONTENT

### ■ Supporting Information

Further experimental details of STM, effusion experiments, and UV-vis absorption spectroscopy. STM image of ordered 9A solvent monolayer. Computational details and further MM results on TPA, 9A, and combined structures. Thermodynamics of TPA dimers in solution. This material is available free of charge via the Internet at <http://pubs.acs.org>.

## ■ AUTHOR INFORMATION

### Corresponding Author

markus@lackinger.org

### Notes

The authors declare no competing financial interest.

## ■ ACKNOWLEDGMENTS

The Nanosystems-Initiative-Munich (NIM) Cluster of Excellence and the China Scholarship Council are gratefully acknowledged for funding. The Warwick Centre for Scientific Computing is acknowledged for providing computing resources.

## ■ REFERENCES

- (1) Datta, A.; Pati, S. K. *Chem. Soc. Rev.* **2006**, *35*, 1305–1323.
- (2) Lehn, J. M. *Rep. Prog. Phys.* **2004**, *67*, 249–265.
- (3) Lehn, J. M. *Angew. Chem., Int. Ed.* **1990**, *29*, 1304–1319.
- (4) Moradian-Oldak, J.; Leung, W.; Fincham, A. G. *J. Struct. Biol.* **1998**, *122*, 320–327.
- (5) Albrecht, M. *Chem. Soc. Rev.* **1998**, *27*, 281–287.
- (6) Knoll, W.; Zizlsperger, M.; Liebermann, T.; Arnold, S.; Badia, A.; Liley, M.; Piscevic, D.; Schmitt, F. J.; Spinke, J. *Colloid Surf. A-Physicochem. Eng. Asp.* **2000**, *161*, 115–137.
- (7) Piot, L.; Silly, F.; Tortech, L.; Nicolas, Y.; Blanchard, P.; Roncali, J.; Fichou, D. *J. Am. Chem. Soc.* **2009**, *131*, 12864.
- (8) Bigioni, T. P.; Lin, X. M.; Nguyen, T. T.; Corwin, E. I.; Witten, T. A.; Jaeger, H. M. *Nat. Mater.* **2006**, *5*, 265–270.
- (9) De Feyter, S.; De Schryver, F. C. *Chem. Soc. Rev.* **2003**, *32*, 139–150.

- (10) Wan, L.-J. *Acc. Chem. Res.* **2006**, *39*, 334–342.
- (11) Lackinger, M.; Heckl, W. M. *Langmuir* **2009**, *25*, 11307–11321.
- (12) Elemans, J.; Lei, S. B.; De Feyter, S. *Angew. Chem., Int. Ed.* **2009**, *48*, 7298–7332.
- (13) Bouteiller, L. In *Hydrogen Bonded Polymers*; Binder, W., Ed.; Springer-Verlag Berlin: Berlin, 2007; Vol. 207, p 79–112.
- (14) Friesen, B. A.; Bhattarai, A.; Mazur, U.; Hippias, K. W. *J. Am. Chem. Soc.* **2012**, *134*, 14897–14904.
- (15) Lei, S. B.; Tahara, K.; De Schryver, F. C.; Van der Auweraer, M.; Tobe, Y.; De Feyter, S. *Angew. Chem., Int. Ed.* **2008**, *47*, 2964–2968.
- (16) Meier, C.; Roos, M.; Kunzel, D.; Breitruck, A.; Hoster, H. E.; Landfester, K.; Gross, A.; Behm, R. J.; Ziener, U. *J. Phys. Chem. C* **2010**, *114*, 1268–1277.
- (17) Kampschulte, L.; Werblowsky, T. L.; Kishore, R. S. K.; Schmitt, M.; Heckl, W. M.; Lackinger, M. *J. Am. Chem. Soc.* **2008**, *130*, 8502–8507.
- (18) Gutzler, R.; Sirtl, T.; Dienstmaier, J. F.; Mahata, K.; Heckl, W. M.; Schmitt, M.; Lackinger, M. *J. Am. Chem. Soc.* **2010**, *132*, 5084–5090.
- (19) Dienstmaier, J. F.; Mahata, K.; Walch, H.; Heckl, W. M.; Schmitt, M.; Lackinger, M. *Langmuir* **2010**, *26*, 10708–10716.
- (20) Bellec, A.; Arrigoni, C.; Schull, G.; Douillard, L.; Fiorini-Debuisschert, C.; Mathevet, F.; Kreher, D.; Attias, A. J.; Charra, F. *J. Chem. Phys.* **2011**, *134*.
- (21) Groszek, A. J. *Proc. R. Soc. London A, Math. Phys. Sci.* **1969**, *314*, 473–498.
- (22) Tahara, K.; Furukawa, S.; Uji-i, H.; Uchino, T.; Ichikawa, T.; Zhang, J.; Mamdouh, W.; Sonoda, M.; De Schryver, F. C.; De Feyter, S.; Tobe, Y. *J. Am. Chem. Soc.* **2006**, *128*, 16613–16625.
- (23) Yang, Y. L.; Wang, C. *Curr. Opin. Colloid Interface Sci.* **2009**, *14*, 135–147.
- (24) Jahanbekam, A.; Vorpahl, S.; Mazur, U.; Hippias, K. W. *J. Phys. Chem. C* **2013**, *117*, 2914–2919.
- (25) Stepanow, S.; Strunskus, T.; Lingenfelder, M.; Dmitriev, A.; Spillmann, H.; Lin, N.; Barth, J. V.; Wöll, C.; Kern, K. *J. Phys. Chem. B* **2004**, *108*, 19392–19397.
- (26) Clair, S.; Pons, S.; Seitsonen, A. P.; Brune, H.; Kern, K.; Barth, J. V. *J. Phys. Chem. B* **2004**, *108*, 14585–14590.
- (27) Canas-Ventura, M. E.; Klappenberger, F.; Clair, S.; Pons, S.; Kern, K.; Brune, H.; Strunskus, T.; Wöll, C.; Fasel, R.; Barth, J. V. *J. Phys. Chem. Phys.* **2006**, *125*.
- (28) Lackinger, M.; Griessl, S.; Kampschulte, L.; Jamitzky, F.; Heckl, W. M. *Small* **2005**, *1*, 532–539.
- (29) Lackinger, M.; Griessl, S.; Markert, T.; Jamitzky, F.; Heckl, W. M. *J. Phys. Chem. B* **2004**, *108*, 13652–13655.
- (30) Prauzner-Bechcicki, J. S.; Godlewski, S.; Tekiel, A.; Cyganik, P.; Budzioch, J.; Szymonski, M. *J. Phys. Chem. C* **2009**, *113*, 9309–9315.
- (31) Martsinovich, N.; Troisi, A. *J. Phys. Chem. C* **2010**, *114*, 4376–4388.
- (32) Fortuna, S.; Troisi, A. *J. Phys. Chem. B* **2010**, *114*, 10151–10159.
- (33) Pinder, J. W.; Richards, F. M. *J. Comput. Chem.* **1987**, *8*, 1016–1024.
- (34) Allinger, N. L.; Yuh, Y. H.; Lii, J. H. *J. Am. Chem. Soc.* **1989**, *111*, 8551–8566.
- (35) Lii, J. H.; Allinger, N. L. *J. Comput. Chem.* **1998**, *19*, 1001–1016.
- (36) Mammen, M.; Shakhnovich, E. I.; Deutch, J. M.; Whitesides, G. M. *J. Org. Chem.* **1998**, *63*, 3821–3830.
- (37) Gutzler, R.; Heckl, W. M.; Lackinger, M. *Rev. Sci. Instrum.* **2010**, *81*, 015108.
- (38) Dejong, A. M.; Niemantsverdriet, J. W. *Surf. Sci.* **1990**, *233*, 355–365.
- (39) Gilli, G.; Bellucci, F.; Ferretti, V.; Bertolasi, V. *J. Am. Chem. Soc.* **1989**, *111*, 1023–1028.
- (40) Allen, G.; Watkinson, J. G.; Webb, K. H. *Spectrochim. Acta* **1966**, *22*, 807–814.
- (41) Bailey, M.; Brown, C. J. *Acta Crystallogr.* **1967**, *22*, 387.
- (42) Foloppe, N.; MacKerell, J. A. D. *J. Comput. Chem.* **2000**, *21*, 86–104.

- (43) Bickerstaffe, A. K.; Cheah, N. P.; Clarke, S. M.; Parker, J. E.; Perdigon, A.; Messe, L.; Inaba, A. *J. Phys. Chem. B* **2006**, *110*, 5570–5575.
- (44) Müller, T.; Flynn, G. W.; Mathauser, A. T.; Teplyakov, A. V. *Langmuir* **2003**, *19*, 2812–2821.
- (45) Kampschulte, L.; Werblowsky, T. L.; Kishore, R. S. K.; Schmittel, M.; Heckl, W. M.; Lackinger, M. *J. Am. Chem. Soc.* **2008**, *130*, 8502–8507.
- (46) Furukawa, S.; Tahara, K.; DeSchryver, F. C.; VanderAuweraer, M.; Tobe, Y.; DeFeyter, S. *Angew. Chem., Int. Ed.* **2007**, *46*, 2831–2834.
- (47) Ahn, S.; Matzger, A. J. *J. Am. Chem. Soc.* **2012**, *134*, 3208–3214.
- (48) Miao, X. R.; Xu, L.; Li, Z. M.; Deng, W. L. *J. Phys. Chem. C* **2011**, *115*, 3358–3367.
- (49) Lackinger, M.; Griessl, S.; Heckl, W. M.; Hietschold, M.; Flynn, G. W. *Langmuir* **2005**, *21*, 4984–4988.
- (50) Schaake, R. C. F.; Vanmiltenburg, J. C.; Dekruif, C. G. J. *Chem. Thermodyn.* **1982**, *14*, 763–769.
- (51) Iwahashi, M.; Hachiya, N.; Hayashi, Y.; Matsuzawa, H.; Suzuki, M.; Fujimoto, Y.; Ozaki, Y. *J. Phys. Chem.* **1993**, *97*, 3129–3133.
- (52) Murthy, A. S. N.; Rao, C. N. R. *Appl. Spectrosc. Rev.* **1968**, *2*, 69–191.
- (53) Sirtl, T.; Song, W.; Eder, G.; Neogi, S.; Schmittel, M.; Heckl, W. M.; Lackinger, M. *ACS Nano* **2013**, *7*, 6711–6718.